JOURNAL OF GEOPHYSICAL RESEARCH, VOL. 103, NO. A11, PAGES 26,495–26,506, NOVEMBER 1, 1998

Properties of ELF emissions in the dayside magnetopause

P. Song,[1,2,3] Z. Zhu,[2] C. T. Russell,[3] R. R. Anderson,[4] D. A. Gurnett,[4] K. W. Ogilvie,[5] and R. J. Strangeway[3]

Abstract. We undertake a comprehensive study of the extremely low frequency emissions within the magnetopause current layer using measurements obtained with ISEE 1 spacecraft. Since the emissions vary greatly, both spatially and temporally, to derive meaningful and robust statistical results is challenging. We design an averaging procedure and choose the normalized wave amplitudes for a correlation analysis. Also, we separate the parameters for the correlation with local or global properties. We found that most of the wave power in the current layer is carried by the magnetic field fluctuations, while the electric field carries relatively little energy. These emissions are best correlated with the local magnetic field shear and electron plasma beta. The power increases as the shear and beta increase. The wave is correlated with the global interplanetary magnetic field (IMF) clock angle, although it is weaker than with the local shear. The wave is weakly correlated with the IMF B_z and is not correlated with the electron temperature anisotropy. The correlation of the electric wave field with our chosen parameters is weaker than and varying from that of the magnetic wave field. These ELF emissions have the characteristics of the whistler mode dispersion with an increasing phase velocity above the lower hybrid frequency and with a cutoff at the electron cyclotron frequency. The wavelength is ~20 to 100 km. In a case study, the electric field is polarized nearly perpendicular to the background magnetic field.

1. Introduction

Enhanced emissions in extremely low frequency (ELF), 3 Hz ~ 3 kHz, near the magnetopause have been known for a long time [*Gurnett et al.*, 1979; *Anderson et al.*, 1982; *Tsurutani et al.*, 1981, 1989, 1998; *LaBelle et al.*, 1987]. While much progress was made in understanding ultra low frequency (ULF), < 1 Hz, fluctuations and other large-scale processes in this region, relatively little progress has been made in understanding ELF waves in the last few years. Recently, the importance of these high-frequency waves in cross-scale coupling has been recognized [e.g., *Ashour-Abdalla et al.*, 1995; *Horwitz et al.* 1996]. It is clear that to have a complete understanding of a phenomenon, one must to understand the underlying microphysics. However, the debate over the significance of the high-frequency fluctuations has been ongoing for some time. Some argue that these fluctuations carry almost no energy compared with ULF waves, the static fields, and the plasma. Therefore they argue that the waves play, at most, minor roles in solar wind–magnetosphere coupling. For example, reconnection takes place in most MHD simulations without invoking any specific microphysical process. Numerical resistivity is often allowed to take the place of the microphysics. Furthermore, observations [*Song et al.*, 1993b; *Le et al.*, 1994; *Treumann et al.*, 1995] and kinetic simulations [*Winske and Omidi*, 1995] have shown little evidence of significant cross-field diffusion. Advocates of the significance of these waves, on the other hand, question the bases upon which certain values of parameters, such as the resistivity and viscosity, have been utilized in MHD simulations.

From a data analyst's point of view, a phenomenon is importantly related to a process means when a parameter that best represents the phenomenon is strongly correlated with a parameter that best represents the process, even though the causal relation between the two still needs to be determined by theory. When we designed our study, we carefully examined the physical meaning of each parameter. We realized that the overall importance of a phenomenon is determined, in general, by two orthogonal factors. The first factor is the importance of the role that the phenomenon plays in the process under consideration. The second factor is the importance of the process. Given the smallness of the energy carried by ELF waves, it is unlikely that these waves directly make a significant impact. It is more likely that these waves are important or even crucial locally and that they carry information or act as identifiers for global processes.

There are several possible mechanisms that can result in enhanced wave power at the magnetopause boundary. One possibility is that the changes in the plasma and field parameters at the magnetopause create a minimum in the phase velocity of the waves. To conserve the total energy flux, the amplitude and hence the power are both higher. Another possibility is that the waves are generated at the regions, such as the dayside cusps, that magnetically connect with the magnetopause and propagate along the field. The third possibility is that the waves are generated in or near where they are observed. In the first two situations, because the waves are observed as a result of propagation away from the sources, the observed plasma conditions do not need to be locally unstable

[1]Space Physics Research Laboratory, University of Michigan, Ann Arbor.
[2]High Altitude Observatory, National Center for Atmospheric Research, Boulder, Colorado.
[3]Institute of Geophysics and Planetary Physics, University of California, Los Angeles.
[4]Department of Physics and Astronomy, University of Iowa, Iowa City.
[5]NASA Goddard Space Flight Center, Greenbelt, Maryland.

Copyright 1998 by American Geophysical Union.

Paper number 98JA02396.
0148-0227/98/98JA-02396$09.00

as long as, under these conditions, the waves are not strongly damped. However, few have reported the results of investigation of these possibilities. The local generation mechanism requires the plasma conditions to be unstable to at least one instability. Observations can provide two tests of possible instability: (1) the plasma conditions have to be at least unstable to that instability and more stable to other competing candidates; and (2) the observed wave properties, such as the dispersion relation and polarization, have to be at least not inconsistent with the wave generated by that instability. If a theory is successful, it will, in turn, help us to understand the function and the consequences of the waves.

Several instabilities that generate waves in the ELF range may be present at the magnetopause. The existence of the gradients in plasmas and magnetic field may lead to growth of various drift mode instabilities. Among those, the lower hybrid drift instability (LHDI) [*Lemons and Gary,* 1977; *Gary and Eastman,* 1979; *Huba et al.,* 1981] has been most attractive. The classical electron anisotropy instability [e.g., *Kennel and Petschek,* 1966] may also operate at the magnetopause under certain conditions. When the magnetic field rotates across the magnetopause, the strong current associated with the field shear may be able to drive the instability of whistler modes [*Drake et al.,* 1994; *Drake,* 1995].

Gurnett et al. [1979] and *Anderson* [1982] provided a comprehensive overview of the ELF waves observed at and near the magnetopause. *Anderson et al.* [1982] studied several cases of these waves and provided detailed pictures of some of the waves. *Tsurutani et al.* [1989] studied the ELF waves statistically. They showed that the correlation of the electric component of the waves with parameters, such as local time, latitude, magnitude, and the Z component of the IMF and *Kp* index, is weaker. The maximum correlation coefficient r^2 is 0.183. *Zhu et al.* [1996] reported the preliminary results of another attempt to study the waves statistically. This paper provides more comprehensive discussion and detailed accounts of the investigation of *Zhu et al.*

We first describe the instruments used in this study, followed by examples of the waves at the dayside magnetopause. Then we describe the database, procedure, and results of our statistical study. Finally, we provide the information we gathered through this study about the properties of the waves.

2. Instrumentation

Data used in this study are from three instruments on board ISEE 1 plus solar wind and IMF information from solar wind monitors. The Iowa Plasma Wave Experiment [*Gurnett et al.,* 1978] provides the ELF wave measurements. There are two analyzers in this experiment. A high time resolution spectrum analyzer covers the frequency ranges from 5.62 Hz to 311 kHz with 20 channels of electric field and from 5.62 Hz to 10 kHz with 14 channels of magnetic field. The channels are logarithmically evenly spaced with a bandwidth of ±15%. The sampling rate is 1 s most of the time and at 1/4 s at the high rate. A narrowband sweep frequency receiver covers the frequency range from 100 Hz to 400 kHz, with a frequency resolution of 6.5%. It takes 32 s for a complete frequency scan. Typical proton and electron gyrofrequencies are 1 Hz and 1 kHz, respectively, in the dayside magnetopause. Therefore the spectrum analyzer provides a reasonably good coverage of waves above the proton gyrofrequency. The measurements from the narrowband sweep frequency receiver are used in this study for confirmation but are not presented in this paper.

The ISEE 1 magnetometer [*Russell,* 1978] measures th vector magnetic field every 1/4 s at the lower rate and 1/16 s a the higher rate. Near the dayside magnetopause the uncertainty of the measurements is 1/128 nT and insignificant compared with the level of fluctuations in the background field in this region. These measurements are used to determine the background field. The analyses of the magnetic fluctuations near and below the proton gyrofrequency using magnetometers have been reported elsewhere [Song et al., 1993a].

The high temporal resolution, two-dimensional (2-D) plasma measurements from the ISEE 1 Fast Plasma Experiment are not routinely available. Since the electron properties and processes associated with electrons are more important to the waves we are studying, we use the measurements from the vector electron spectrometer (VES) [*Ogilvie et al.,* 1978]. The VES employed six electrostatic detectors, each with 8.5° x 11° fields of view, looking in each sense along three mutually orthogonal directions fixed in the ISEE 1 spacecraft. The electron energy range at each detector is divided into 16 steps from 11 to 2062 eV. This arrangement provides three-dimensional (3-D) measurements of electrons near the magnetopause covering particles from a variety of sources.

3. Case Studies

Because, as pointed out previously [*Gurnett et al.,* 1979; *Tsurutani et al.,* 1989; *Zhu et al.,* 1996], ELF waves are highly variable both from case to case and within each case, one has t examine many cases before determining the typical behavior o these waves. We present four cases of ISEE 1 magnetopause crossings. Two of them occurred with large magnetic shear across the magnetopause, and the other two occurred with small magnetic shear.

Here are some general guidelines to reading the spectra. If the enhancements appear in both electric and magnetic fields, the waves are electromagnetic. From Faraday's law, loosely speaking, the ratio between the two components is approximately the square of the phase velocity. For example, if the two spectra have a similar slope in a frequency range, the dispersion is weak in this frequency range. If the electric component increases, the phase velocity increases and vice versa. If the enhancements occur only in the electric component, the waves are electrostatic. From Faraday's law the wave vector is parallel to the electric perturbations and the phase velocity cannot be derived by using the ratio between the electric and magnetic amplitudes. In our discussion we refer to "narrowband" waves as those with a distinct peak in the spectrum, and to "broadband" waves as those without such a peak, in particular, without a clear lower cutoff frequency. In general, the waves resonate with particles, either obtaining energy from or giving away energy to particles. The bandwidth of a wave provides an important clue to understanding, for example, the selectiveness of the resonance process.

The dynamic ranges of the gray-scale spectral plots presented in this paper are the same. The gray scale is proportional to the wave intensity times the frequency. The plasma density and the magnetic field strength are presented in terms of the plasma frequency and electron cyclotron frequency, respectively, in the dynamic spectral plots.

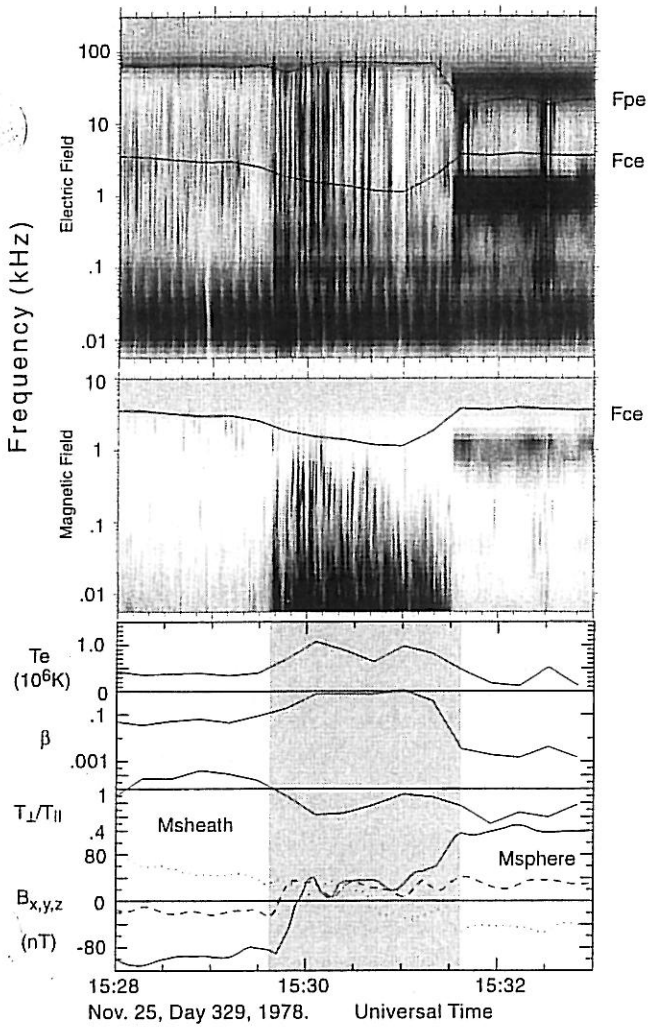

Figure 1. An ISEE 1 inbound subsolar magnetopause crossing with larger field shear. (top) Electric and (middle) magnetic fields measurements from the Iowa Plasma Wave Experiment. The gray scale is proportional to the intensity times the frequency. The electron plasma frequency F_{pe} and cyclotron frequency F_{ce} are calculated from the electron density and magnetic field measurements, respectively. (bottom) Electron temperature T_e, electron plasma beta, $2\mu_0 NkT_e/B^2$, and the electron temperature anisotropy, $T_\perp / T_\parallel$, measured by vector electron spectrometer (VES), and the three components of the background magnetic field in the spacecraft coordinates (B_x, dashed line; B_y, dotted line; and B_z solid line). The magnetopause current layer is from 1529:40 to 1531:40 UT.

November 25, 1978, crossing. This crossing, shown in Figure 1, occurred near the subsolar region during a strongly southward IMF. This is one of the occasions when ISEE 1 registered a clean magnetopause crossing for strongly southward IMF. We recall that during southward IMF, the magnetopause is much more dynamic [*Song et al.*, 1988] and flux transfer events (FTEs) frequently disturb the magnetopause conditions [*Russell and Elphic*, 1979; *Gurnett et al.*, 1979]. The field shear across the magnetopause current layer is close .o 180°. Note that most of the field changes occur at the two edges of the current layer. Within the current layer the field rotates relatively smoothly. There are two striking types of wave activity during this crossing, best seen in the magnetic component. One is broadband emission in the lower- and middle-frequency range, present in the region where the background magnetic field undergoes its change from the magnetosheath field to the magnetospheric field from 1529:40 to 1531:40 UT. The other is narrowbanded on the magnetospheric side, with frequencies a fraction of the electron cyclotron frequency. Note how sharp the termination of one wave and the start of the other is. This may indicate a change in magnetic topology. The absence of the lower-frequency emissions in the narrowband waves indicates the lack of the high-energy electrons that travel along the field. Here we recall that particles of higher energies resonate with electromagnetic waves of lower frequencies. This therefore can be used as the diagnostics of trapped particles on closed field lines [*Song et al.*, 1993b]. The focus of this study is on the waves within the current layer.

Figure 2 compares spectra in each region. The wave power in the current layer (solid lines) is highest in a broad range up to 0.3 kHz. Above 3 kHz the power in either the electric or magnetic component in the current layer is not higher than the power in the magnetosphere and magnetosheath; indicating no significant wave activity in the current layer in the high-frequency range. In the current layer the field strength is 88 nT, which translates to an electron cyclotron frequency of 2.5 kHz and a lower hybrid frequency of 57 Hz. Below 10 Hz (three channels below the lower hybrid frequency) the electric component is significantly weaker, indicating a lower phase velocity. From 10 Hz to 1 kHz (note that the electron cyclotron frequency is between this and the next channels) the two spectra tend to converge, indicating an increase in the phase velocity. Higher than 1 kHz, the two spectra start diverging and hence the phase velocity decreases again. The peak shown in the spectra of the magnetospheric side corresponds to the narrowband electromagnetic wave. The difference between the two spectra at this peak is much less than those in the current layer, indicating that this narrowband

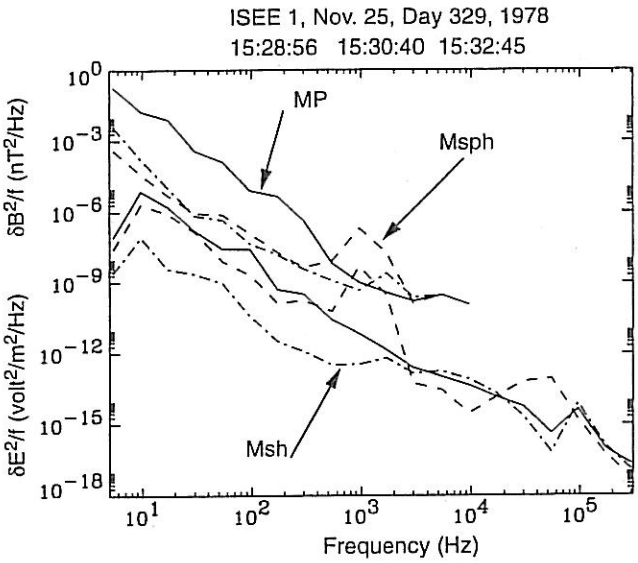

Figure 2. The spectra from the magnetosheath, current layer (solid lines), and magnetosphere for the crossing shown in Figure 1. The top three traces are the magnetic component, and the bottom three are electric. Msh, MP, and Msph denote the magnetosheath, magnetopause current layer, and magnetosphere, respectively.

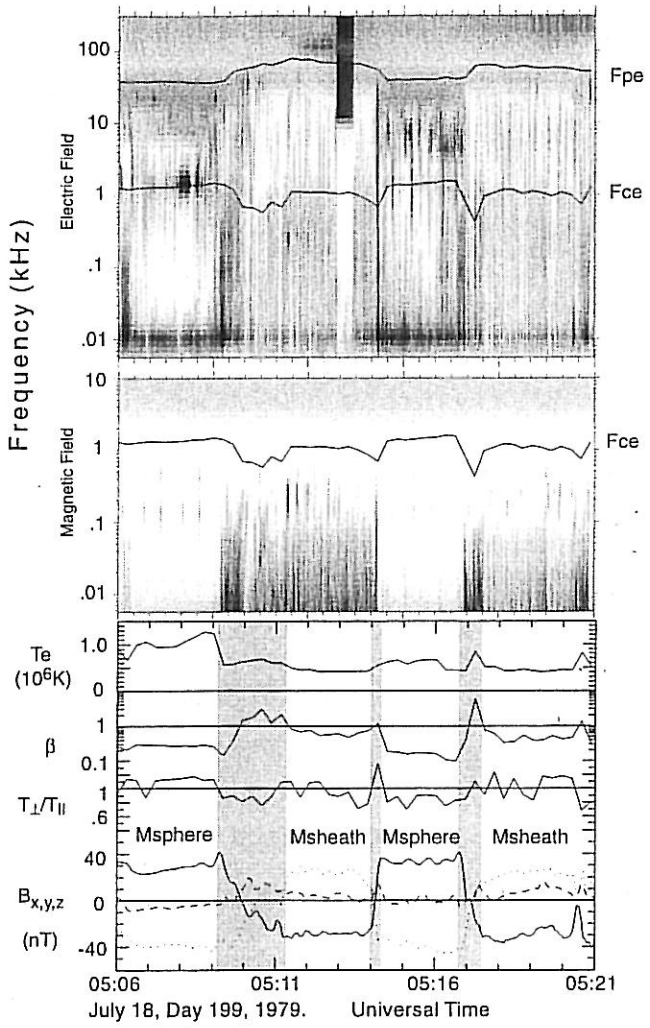

Figure 3. An ISEE 1 outbound pass with large field shear in the same format as Figure 1. Three current layer crossings occur at near 0510, 0514, and 0517 UT.

wave propagates more quickly than the waves in the current layer. The electric field enhancements at the highest frequencies for each spectrum are associated with the oscillations at the plasma frequency and upper hybrid frequency.

Within the magnetopause current layer, where the electromagnetic emissions are enhanced, are increases in the electron temperature, ion temperature and fluctuations below the proton cyclotron frequency [*Song et al.*, 1993a]. The electron plasma beta, the ratio of the electron thermal pressure to the magnetic pressure, has a clear correlation with the presence of the broadband waves, while the electron temperature anisotropy does not show any unusual behavior. Within the current layer the density (see the plasma frequency in Figure 1) is constant, changing abruptly upon entering the magnetosphere; indicating that it is unlikely that there are significant diffusive processes.

July 18, 1978, pass. Figure 3 shows a rather typical large shear case. There are a few crossings during the present interval. The rotation of the field across the magnetopause current layer is about ~170°. The internal structure of the current layer is not clearly resolvable, perhaps owing to the fast motion of the current layer relative to the satellite and the limited temporal resolution of the data. The magnetic component of the waves in the magnetosheath is not as weak as in the first case, while the power is further enhanced at t' field rotations. The narrowband electromagnetic emissions the magnetosphere are not present. Instead, there are some electrostatic enhancements near the electron cyclotron frequency in this region. Comparison of the spectra in different regions (see Figure 4) shows the same pattern as that of Figure 2; the magnetic noise is enhanced within the current layer. However, in this case, the magnetosheath electric noise is more intense at frequencies higher than 30 Hz, and below 30 Hz it is similar in intensity to the magnetospheric level. Thus there is no significant electric component of the wave activity in the current layer. At the lowest frequencies the electric wave power decreases in the current layer. As in the first case, the electron temperature in the current layer is higher than in the magnetosheath, the electron plasma beta is higher at the field rotation and where the wave is strong, and the electron temperature anisotropy does not seem to correlate with the wave enhancements.

November 1, 1978, crossing. This magnetopause crossing, shown in Figure 5, is one of the best documented ISEE magnetopause crossings [*Song et al.*, 1993; *Ogilvie and Fitzenreiter*, 1989]. The crossing occurred at the subsolar point with very small magnetic shear across the magnetopause. In the current layer or the sheath transition layer referred to by Song et al., the electron temperature is not higher than in the magnetosheath, in contrast to the previous two high shear cases. The electron beta does not increase in the sheath transition layer from its magnetosheath value. In fact, it decreases. The wave activity in the sheath transition layer remarkably weaker than that of the high shear cases. Th magnetosheath and magnetospheric boundary layers are also significantly quiet in the magnetic component. Additional wave activity occurs in the magnetosheath; electromagnetic emissions at low frequencies in association with the density (magnetic field strength) increase (decrease). These waves have been referred to as lion roars [*Smith et al.*, 1969; *Smith and*

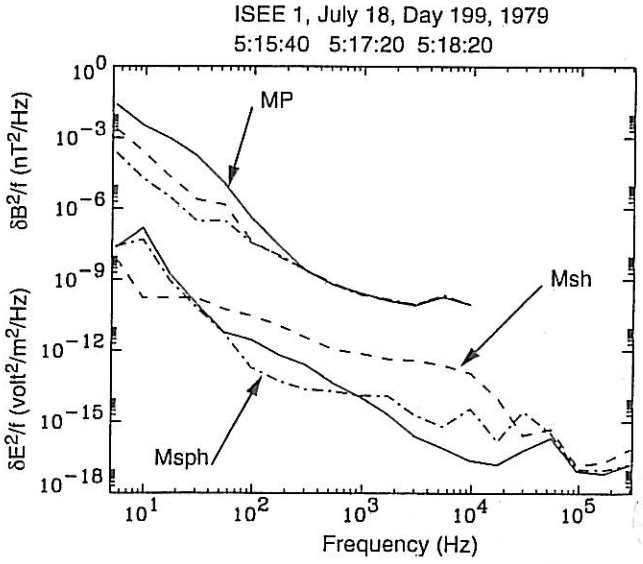

Figure 4. Spectra, in the same format as Figure 2, from the crossing shown in Figure 3.

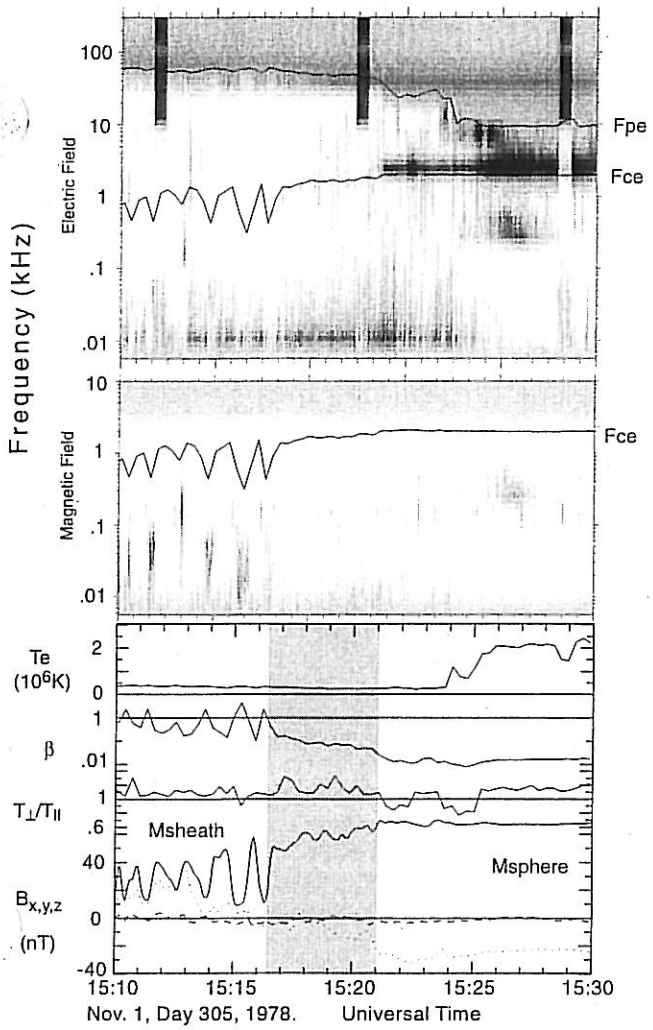

Figure 5. An ISEE 1 inbound crossing with small field shear in the same format as Figure 1.

Tsurutani, 1976; *Tsurutani et al.,* 1981]. On the magnetospheric side there is a distinct electrostatic wave at about $3/2F_{ce}$, where F_{ce} is the electron cyclotron frequency. This type of the wave has been studied elsewhere [*Kennel et al.,* 1970; *Kurth et al.,* 1979; *Gurnett et al.,* 1979] and is interpreted as being generated by a mixture of a cold population (presumably from the ionospheric photoelectrons) with a hot population (presumably from the magnetospheric trapped electrons) [e.g., *Kennel and Ashour-Abdalla,* 1982]. One of the most important features of this wave is its abruptness when appearing, indicating distinct changes in the plasma population and topology. A narrowband electromagnetic wave similar to that of the first case occurs in the magnetosphere, but it seems to be more limited in space. Comparing the spectra (Figure 6) does not show any significant wave activity in the sheath transition layer through the whole frequency range. The three magnetic spectra are near the noise level of the sensor. The peak in the electric component of the nagnetospheric wave near 3 kHz is an example of electrostatic spectra that show no evidence for enhancements in the magnetic component. Again, at the lowest frequencies the electric wave power decreases.

August 20, 1979, crossing. This randomly selected, small-shear case is illustrated in Figure 7. On this outbound pass the field rotates but a few degrees across the magnetopause. The shaded region is where the field changes from the magnetosheath to the magnetospheric one or the magnetopause current layer, although the current is extremely weak. The wave activities in this case are somewhat similar to the last case as follows: narrowband electromagnetic wave below the electron cyclotron frequency in the magnetosphere, the $3/2F_{ce}$ electrostatic wave in the magnetosphere with a somewhat lower frequency but extended into the sheath transition layer; and an absence of the broadband electromagnetic waves in the sheath transition layer. The lion roars and the slow oscillations in the density and field strength in the magnetosheath, however, do not appear in this case. In our previous studies we have suggested using the name "sheath transition layer" for the current layer region under such circumstances in order to emphasize the importance of the changes in plasma properties. This case is interesting because it demonstrates that to identify the magnetopause as a single point can be misleading and such a single point highly depends on the measurement used. For example, if one defines the "magnetopause" to occur at 1343:20 UT according to the plasma data, then the electrostatic wave above the electron cyclotron frequency will extend into the magnetosheath. However, according to plasma theory [*Kennel and Ashour-Abdalla,* 1982], this wave is an indicator of a topological change and the presence of ionospheric photoelectrons. The field lines in this region connect with the ionosphere. A comparison of the spectra (see Figure 8) shows no wave enhancement in the sheath transition layer, although there seems to be an electrostatic wave near the electron cyclotron frequency.

Summary. We have shown a pair of ideal cases and a pair of more "typical" cases for large and small shears, respectively. Figure 9 compares the spectra within the current layer for each case. From these four cases the following is found to be generally true.

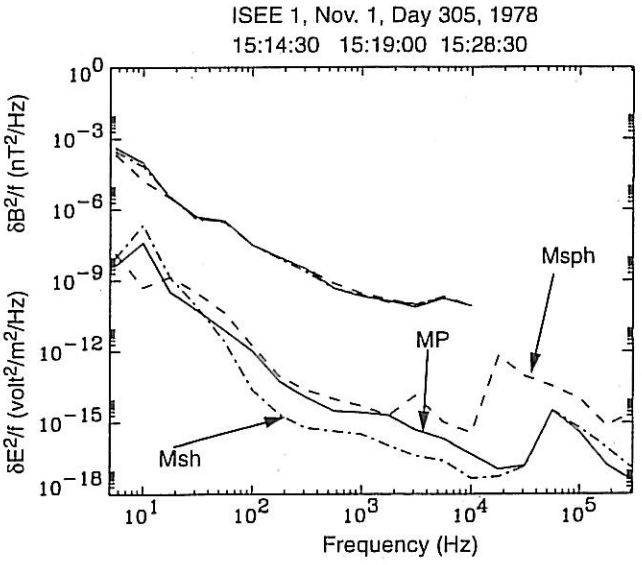

Figure 6. Spectra of the crossing in Figure 5, in the same format as Figure 2.

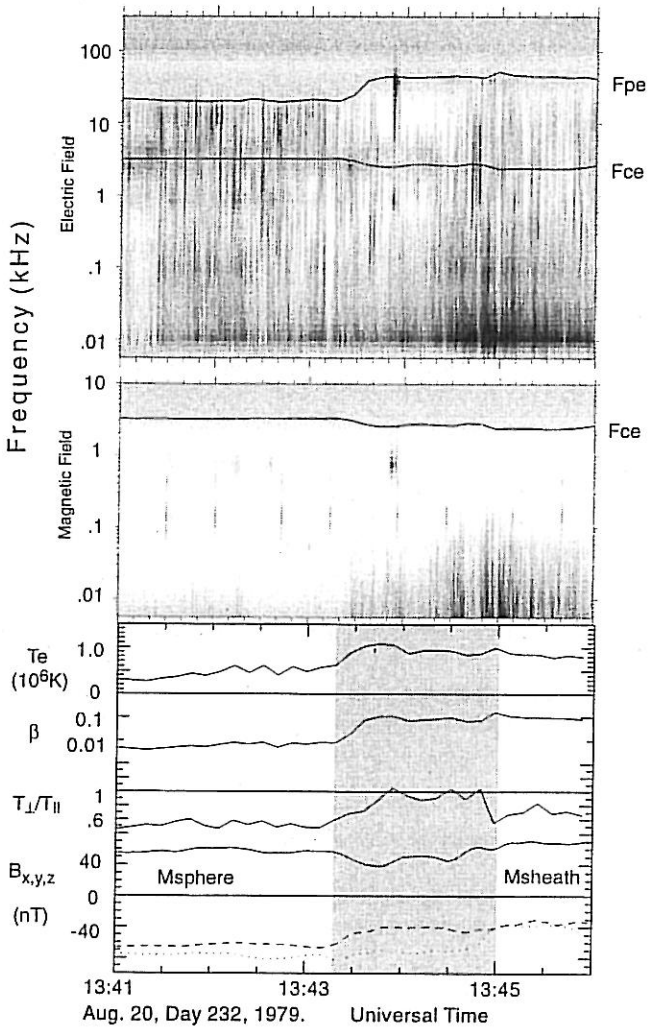

Figure 7. An ISEE 1 outbound crossing with small field shear in the same format as Figure 1.

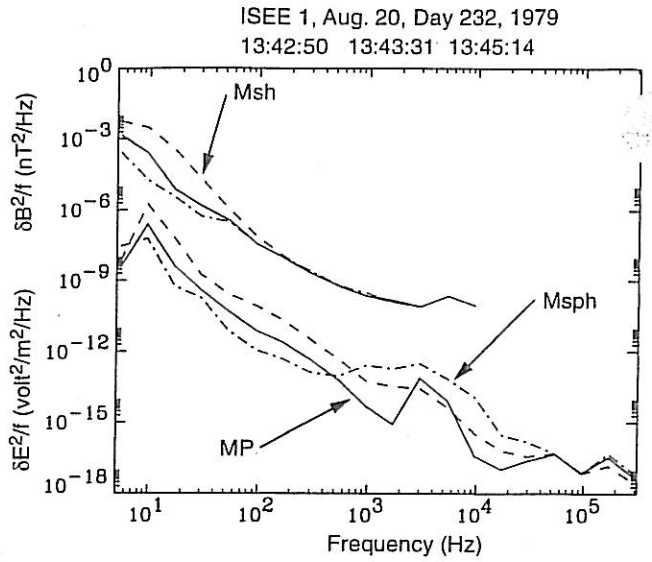

Figure 8. Spectra of the crossing in Figure 7, in the same format as Figure 2.

4. Statistical Study

We have surveyed the magnetopause crossings during the entire ISEE period [*Petrinec et al.*, 1991; *Shue et al.*, 1997]. We compiled a database of those dayside crossings when Iowa Plasma Wave Experiment, vector electron spectrometer, ISEE 1 magnetometer, and solar wind and IMF data from either ISEE 3 or IMP 8 are available. Crossings coinciding with FTEs, partial crossings, and crossings that cannot be clear identified owing to high-level fluctuations at the time of t crossing are excluded from the selection. Furthermore, we include only crossings with a duration longer than 16 s, which is the temporal resolution of the vector electron spectrometer, so that we have at least one VES sample within the current layer. There are totally 265 crossings from 130 passes in this database. The locations of these passes are shown in Figure 10. The coverage of our database is mostly at lower latitudes and partially at midlatitudes over the dayside.

1. The ELF waves in the magnetopause current layer increase in amplitude with the magnetic shear across the magnetopause current. For large shears the waves can be stronger than those on either side of the current layer.

2. The enhanced waves have a strong magnetic component and hence are electromagnetic modes. The electric power in the current layer may or may not be higher than that in either the magnetosheath or magnetosphere.

3. The enhanced waves are relatively broadbanded below the electron cyclotron frequency. The electric wave power often drops at the lowest frequencies, although the magnetic power does not.

4. The electron temperature in the current layer is often higher than that in the sheath if the waves are enhanced.

5. An enhanced electron plasma beta close to or greater than unity is usually associated with the enhanced waves. When the electron plasma beta is significantly less than unity, waves are weak.

6. There is no clear correlation of the wave enhancements with the electron temperature anisotropy.

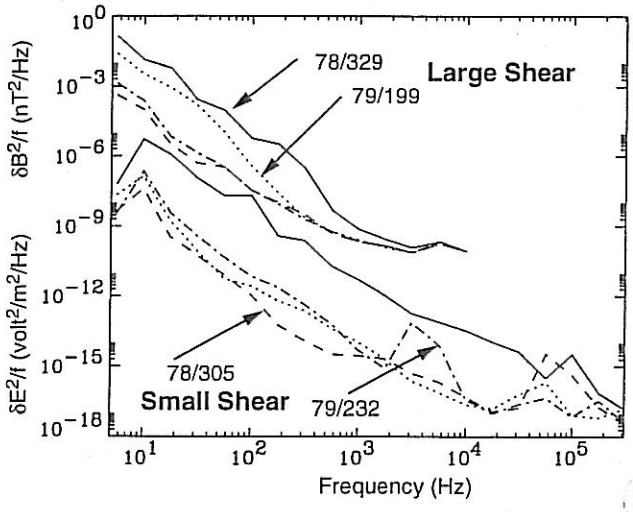

Figure 9. Comparison of the spectra of the current layer from the four cases shown in Figures 1, 3, 5, and 7.

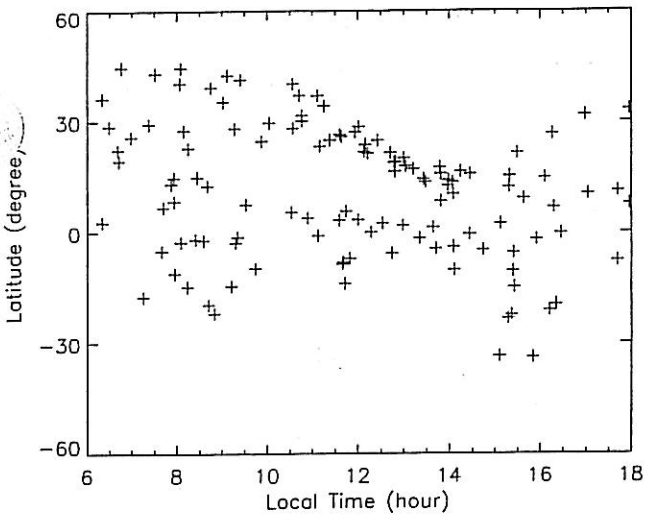

Figure 10. Locations in GSM coordinates of the magnetopause passes used in this study.

For each crossing we take two points, one at the outer edge and one at the inner edge of the current layer, and then record the two field values, $\mathbf{B}_1$ and $\mathbf{B}_2$, and the algebraic averages of magnetic field $\mathbf{B}_0$ and other plasma parameters between the two points. The shear angle is defined as $\vartheta_{sh} = \cos^{-1}[(B_1 \bullet B_2) / (|B_1||B_2|)]$. The normalized wave amplitudes dE/B_0 and dB/B_0 are derived by first geometrically averaging the corresponding power of the measurements over the period between the two points, then integrating over the frequency, taking its square root to obtain the amplitude, and finally normalizing it by the strength of the background magnetic field B_0. The normalized amplitudes are binned according to each parameter with which a correlative analysis is performed in this study. A geometrical mean is derived from a bin with 50% overlap with its neighboring bin on each side. An error bar indicates the probable error of the mean. Here we want to emphasize that the averaging procedure is technically important to ensure the quality of our results. The geometrical mean is critical to correctly represent the average of fluctuations of large magnitude.

The solar wind and IMF data are shifted by x/v_{sw} to account for the convection time from the solar wind monitor to ISEE 1, where x is the distance between the two spacecraft in the x direction and v_{sw} is the simultaneous solar wind velocity.

In the following we study the correlation between the wave amplitudes and each parameter of interest. When exercising such an analysis, one may find that sometimes the correlation derived from the electric component differs from that of the magnetic component. In this case one needs to decide which correlation is more meaningful. For electromagnetic modes the ratio of the energy densities of the electric and magnetic fields of the wave is $\varepsilon_0 dE^2/(dB^2/\mu_0) = dE^2/(dB^2c^2)$. In our system of units, dE in volts per meter and dB in nanoteslas, the electric component dE is significant if $dE/B_0 \sim dB/B_0 \times 3 \times 10^5$ (kilometers per second). In our presentation we use 10^4 km/s as the unit of dE/B_0. In these units, dE/B_0 needs to be 30 times greater than dB/B_0 to be of significance. However, as we will see, the electric field carries little energy in the wave we are studying. Therefore we use the magnetic field as the diagnostics of the correlation. A differing correlation of the electric component may indicate changes in the wave properties, for example, the phase velocity, with the correlating parameter. This argument does not apply to electrostatic waves. Ideally, the magnetic component of an electrostatic wave is zero. The measured magnetic power, if significant, may be due to fluctuations generated by different mechanisms, should not be correlated with the electric wave power, and hence should be considered as noise in the study. As shown in the examples, fortunately, there is no significant electrostatic enhancement in the magnetopause current layer other than a narrowband wave in one of the small shear cases.

There are two important aspects when choosing a parameter to correlate with the wave power. The first is to choose either a global or local parameter, as explained in section 1. The second is to choose a parameter in its normalized or unnormalized form. The IMF B_z is an example of global unnormalized parameters, while the IMF clock angle is its normalized form.

Figure 11 shows the correlation of the wave amplitudes with the local magnetic shear ϑ_{sh} and IMF clock angle. The IMF

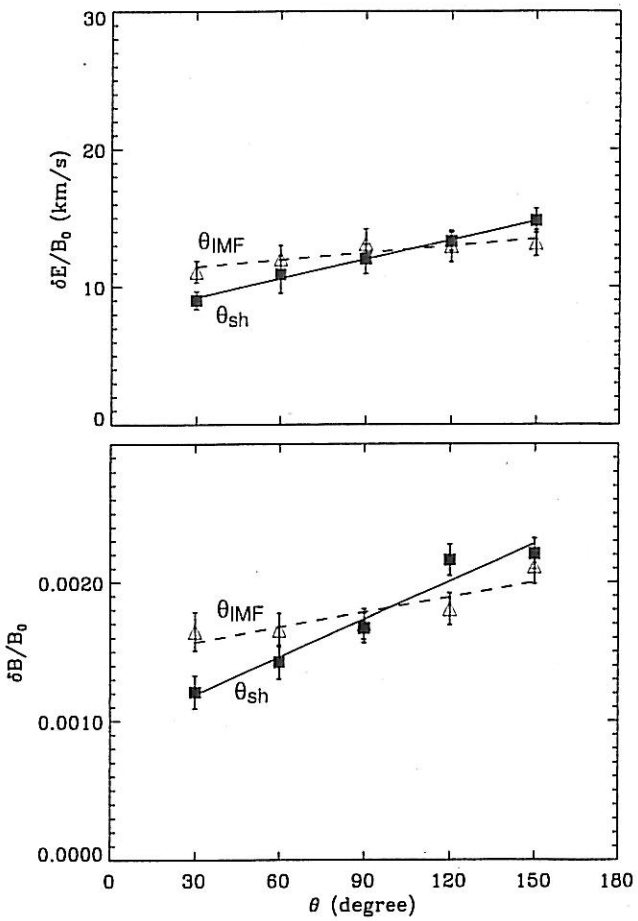

Figure 11. The correlation of the (top) magnetic and (bottom) electric amplitudes of the ELF wave normalized by the background magnetic field strength with the shear angle across the current layer (squares and solid lines) and IMF clock angle (triangles and dashed lines). The symbols are bin averages. The error bars are the probable error of means. The lines are linear fits.

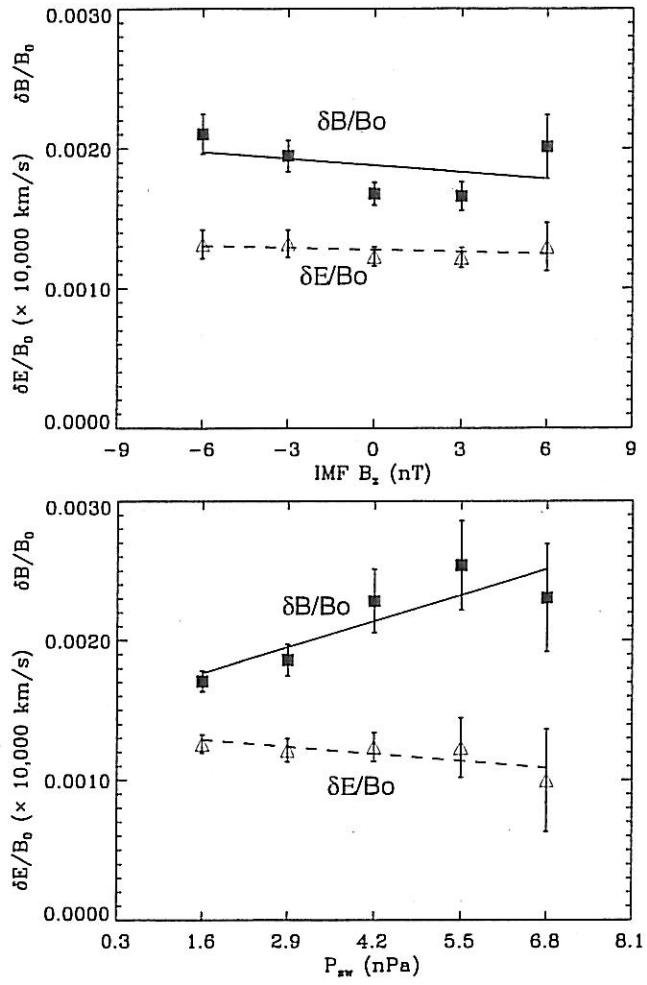

Figure 12. The correlation of the normalized magnetic (squares and solid lines) and electric (triangles and dashed lines) amplitudes with the z component of the IMF (top) in the GSM coordinates and (bottom) the solar wind dynamic pressure.

clock angle, the angle between the yz components of the IMF and north, is the most important measure of reconnection in global context, whereas the local magnetic shear is the indicator of reconnection in the local context. The clear correlation of both electric and magnetic wave amplitudes with the local shear angle, but less clear correlation with the IMF clock angle indicate that these ELF emissions are most likely to be related with the reconnection processes at or near the reconnection sites. One possible interpretation is that these waves are important locally for reconnection to take place but are not strongly related to global processes. An alternative interpretation is that the waves are a by-product of reconnection and may not play an important role in reconnection.

Figure 12(top) shows the correlation of the wave amplitude with the north-south component of the IMF. The correlation between the IMF B_z and either the electric or magnetic wave amplitude is weak. One can see that the correlation with such an unnormalized global quantity is not as good as that with a normalized quantity, such as the clock angle shown in Figure 11. Figure 12(bottom) shows the correlation with the solar wind pressure. The weak correlation between the electric component and B_z is consistent with *Tsurutani et al.*, [1989]. The magnetic component of the wave seems to have a positive correlation with the solar wind pressure, whereas the electric component may be inversely correlated with the solar wir pressure. Here we caution against the simple interpretati that directly links a mechanism with the wave because the wave may be a by-product of other processes.

As we have repeatedly seen in the examples of a correlation between the wave and the electron plasma beta, we show the statistical relationship between the two in Figure 13(top). There is an excellent linear correlation between the logarithm of the beta and the magnetic amplitude, but the correlation of the beta with the electric field is weak.

The temperature anisotropy $T_\perp / T_\parallel$ is one of the possible sources of free energy. Figure 13(bottom) shows the relationship of the wave amplitudes and the electron anisotropy. Often, the anisotropy is less than 1. There is no clear correlation between the magnetic component of the wave with the anisotropy, whereas the electric component is anticorrelated with the anisotropy. Namely, the electric field perturbation is stronger when the parallel temperature of the electron is greater than the perpendicular temperature. However, here we need to point out that the temperature

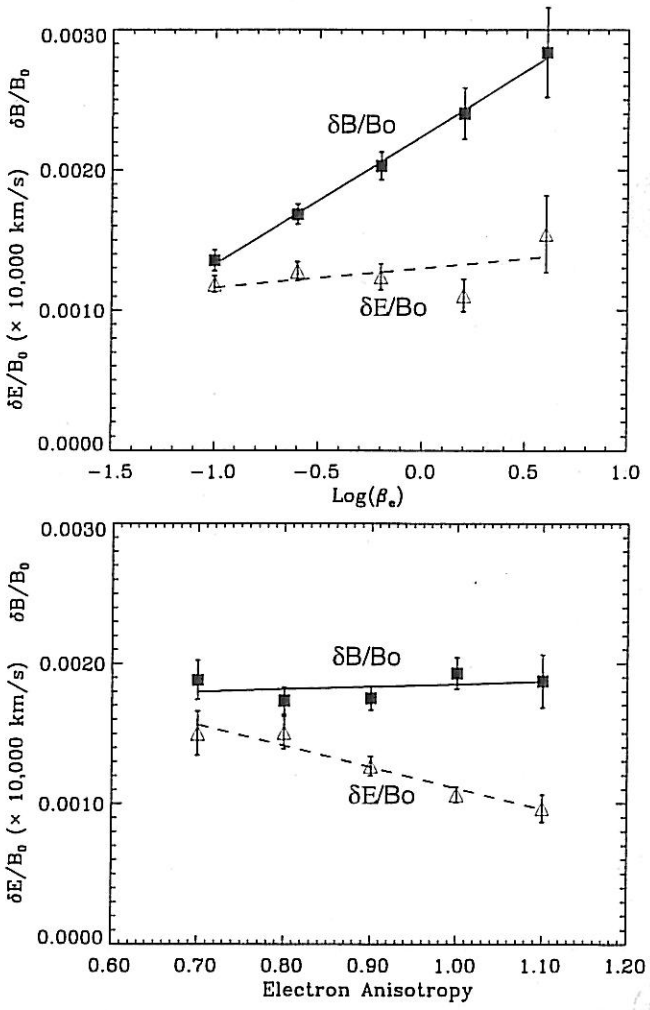

Figure 13. The correlation of the normalized magnetic (squares and solid lines) and electric (triangles and dashed lines) amplitudes with (top) the electron plasma beta and (bottom) the electron temperature anisotropy.

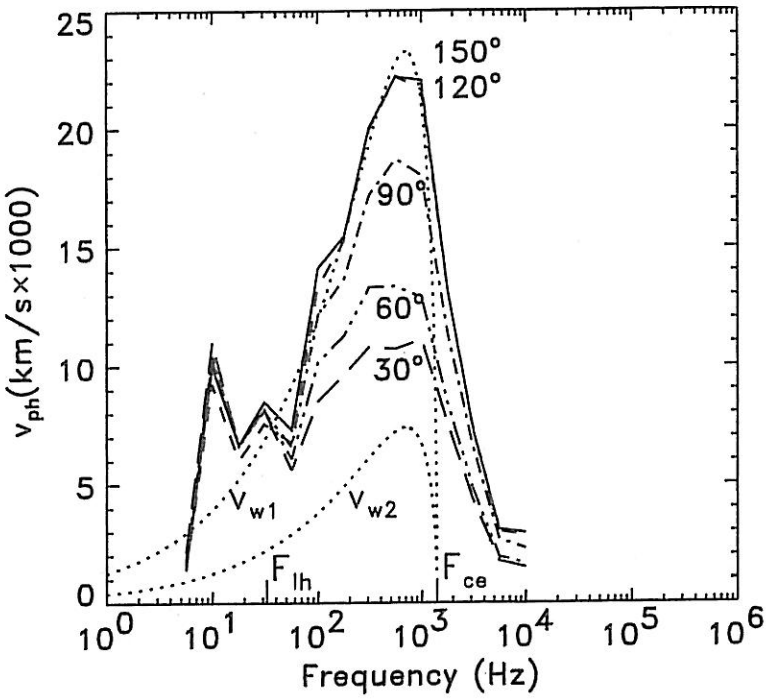

Figure 14. Dispersion relation of the waves in the current layer as functions of the field shear angle [*Zhu et al.*, 1996]. F_{lh} and F_{ce} are the lower hybrid and electron cyclotron frequencies, respectively, derived using the average field strength measured in this region. The two dotted lines, v_{w1} and v_{w2}, are theoretical dispersion curves of parallel propagation whistler modes with a magnetic field strength of 50 nT. Here v_{w2} is derived using average density measured in this region, but v_{w1} uses a density 10 times lower, while the latter provides an impressive fit to the observed dispersion relation of high shears. The factor 10 is much greater than any known uncertainty of the measurements.

anisotropy derived from the VES is based on particles below 2 keV. As the contribution from higher energy particles is important to the temperature measurements (because they are the second moment) and the anisotropy of the higher-energy particles can be greater than 1, caution has to be taken when interpreting Figure 13(bottom).

5. Phase Velocity, Wavelength and Polarization

In order to understand the physics associated with these ELF waves, it is important to identify the mode of the waves. *Zhu et al.* [1996] (see reproduction in Figure 14) showed that the dispersion relation of the wave has the characteristics of the whistler mode, namely, a rising tone and a cutoff at the electron cyclotron frequency. Since the phase velocity of our ELF waves is much greater than the flow velocity, $\leq 10^2$ km/s, the Doppler shift is small and hence the measured frequency can be directly used as the wave frequency. However, quantitatively, the calculated phase velocity based on the observed amplitude ratio is more than 3 times greater than that calculated from the parallel propagating whistler mode dispersion relation in cold plasmas. The cause of the difference is not clear yet because of the complexity of various instruments and their calibrations. While it is possible that the difference is caused by instrumentation, physical reasons could also play a role. The two major assumptions made in deriving Figure 14 are (1) the observed phase velocity is defined as the ratio of the two averaged wave fields and (2) the theoretical dispersion relation is based on parallel propagation in cold plasmas. On the observation side, since our database is not small, we believe that the averaged wave field will wash out the effects from different field and spacecraft spin axis orientations. A question remaining is whether the ratio of the two fields equals the phase velocity. From Faraday's law, if the wave electric field is not perpendicular to the wave vector, the ratio of the two wave fields equals the phase velocity divided by sinφ, where φ is the angle between the electric field and the wave vector. If this is the cause of the difference, angle φ needs to be ~20°. As we show next, the wave electric field is nearly perpendicular to the background field if the above is true. On the theoretical side, since the phase velocity of the whistler mode does not strongly depend on the temperature in our parameter range, our cold plasma assumption holds well. However, when the wave propagates obliquely to the background field, the phase velocity decreases with respect to the velocity of parallel propagation. This makes the difference even worse. Therefore, although the observed dispersion relation has the characteristics of whistler modes, it seems there is a quantitative difference between the observed dispersion and that from plasma theory, the source of which is not well understood and needs further investigation.

Using the phase velocity and frequency given in Figure 14, the wavelength can be derived. For waves between the lower hybrid and electron cyclotron frequencies, the wavelength is ~20 to 100 km. For waves of higher frequencies, the wavelength could be as short as 100 m. These are consistent with the estimate of *Anderson et al.* [1982], who compared the signals received by different antennas and concluded that the

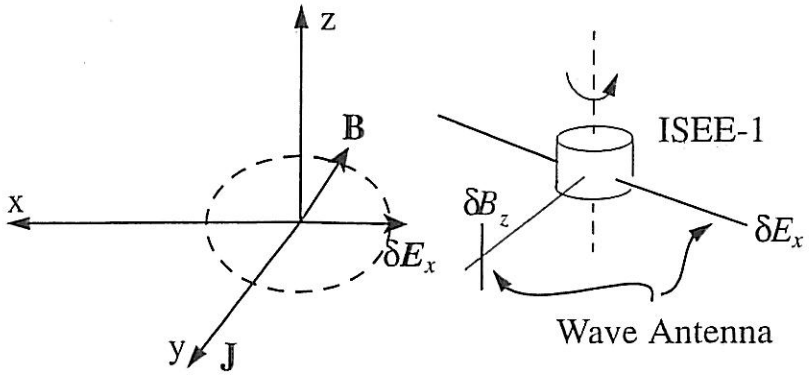

Figure 15. Illustration of the ISEE 1 and its antenna. The spin axis is the z_{sc} direction. The measurements are recorded while the antenna rotates on the xy_{sc} plane. Spin modulation will be seen if the direction without perturbation and the direction with major perturbation are on the xy_{sc} plane.

wavelength is longer than 215 m for waves below 3 kHz and shorter than 215 m for higher-frequency waves.

Next, we investigate the polarization of the waves. As illustrated in Figure 15, the wave power was measured while the spacecraft was spinning, and the two components of the perturbation on the spin plane are measured in time sequence. For waves of wavelength much greater than the satellite's antenna, i.e., 215 m, the signals are spin modulated. The spin modulation is best observed when one of the directions in the spin plane is along the polarization direction and the other is in the direction without any wave perturbation. If the wave is circularly polarized with a different frequency than the spin frequency, the spin modulation is best seen when the spin plane and polarization plane are orthogonal to each other. Since the received signal measures only the strength of the fields and does not recognize the sign of the perturbation, the spin modulation should be at the frequency that is twice of th spin frequency. The ISEE 1 spin period is 3 s. The Iowa Plasm Wave Experiment has two sampling rates, 1 s at the lower rate and 1/4 s at the higher rate. Therefore at the higher sampling rate, the instrument should be able to detect the polarization of the wave perturbation projected on the spin plane. Figure 16 shows one of the magnetopause crossings at such a high rate.

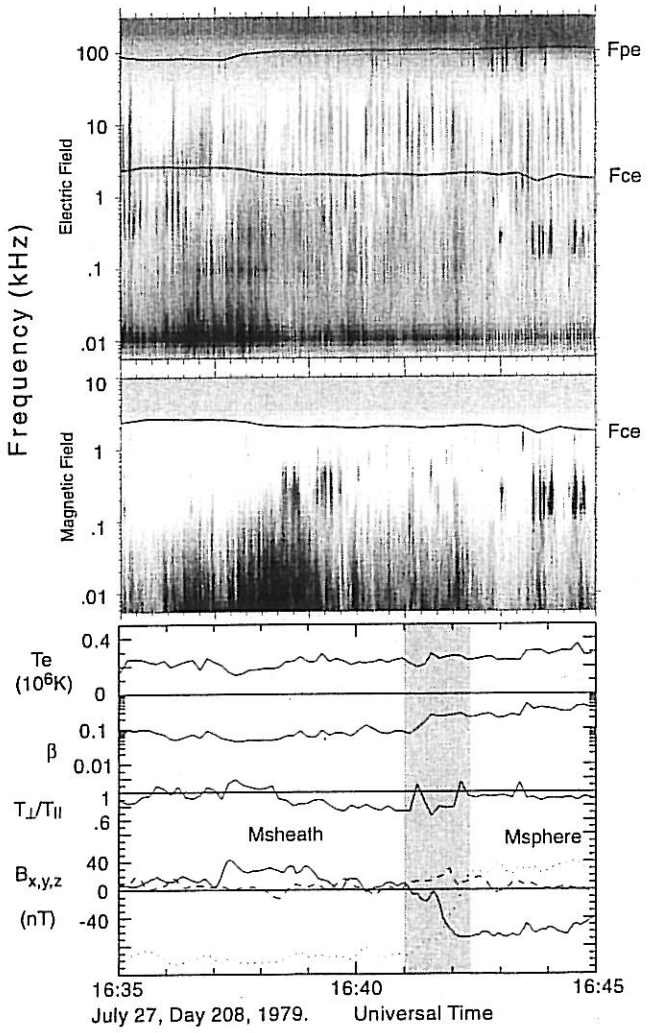

Figure 16. An inbound ISEE 1 magnetopause crossing with large field shear at the high sampling rate, in the same format as Figure 1.

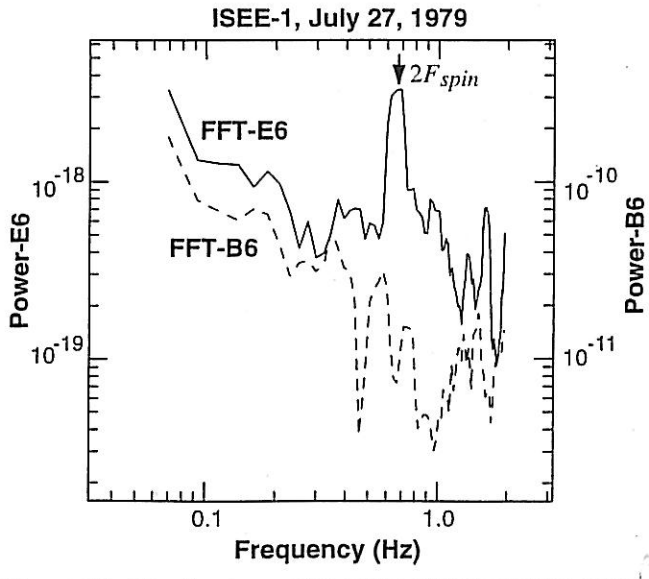

Figure 17. The Fourier spectra of the 100 Hz channel of the electric (solid line) and magnetic (dashed line) signals from 1640:30 to 1641:40 UT during the crossing shown in Figure 15.

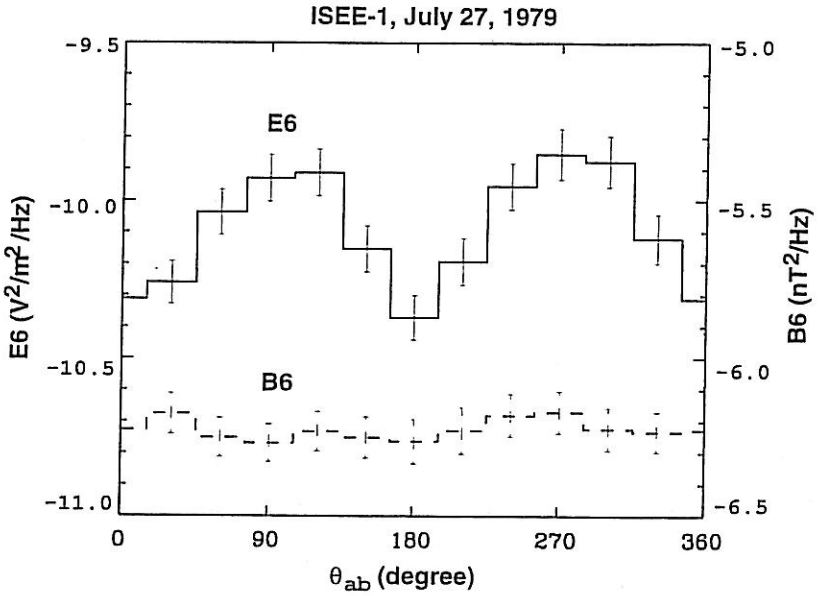

Figure 18. Bin averages of the 100 Hz channel electric (solid line) and magnetic (dashed line) signals as functions of the angle between the antenna and background magnetic field projected on the spin plane. The error bars are the probable error of means.

Figure 17 shows the Fourier analysis of the time series of the electric and magnetic signals from the 100 Hz channel. During the interval the electric signals measured the components on the spin plane while the magnetic signals measured along the spin axis. There is a clear peak in the electric field at 0.67 Hz. We note the possibility that this peak could be due to ULF waves instead of spin-modulation. The absence of such a peak in the magnetic field channel makes it unlikely that the 0.67 Hz peak is not due to the spin modulation rather than other possible ULF wave sources. Here we recall that most ULF waves below the proton gyrofrequency, 1 Hz in this case, are electromagnetic. Therefore the enhancement of the electric power at 0.67 Hz should not be due to ULF waves at this frequency because, otherwise, it should have a significant magnetic component, which is not observed. We plot in Figure 18 the wave measurements as functions of the angle between the ambient magnetic field projected on the spin plane and the direction of the antenna. The electric field is strongest when the antenna is 90° to 120° and 270° to 300° with respect to the background field. It is most likely that the electric field is perpendicularly polarized, although it may have a small component along the background field. For this case the wave electric field is along x, and the electric current and the background magnetic field, in the yz plane, are more or less along each other. The polarization of the magnetic field cannot be determined using this method in this case because the search coil is aligned along the spin axis.

6. Conclusions and Discussion

Although ELF emissions are highly temporally/spatially varying, even during the same magnetopause crossing, there is a clear correlation of the ELF waves with the field shear across the magnetopause. Broadband electromagnetic waves, from 10 Hz to 1 kHz, are enhanced with the increase in the local shear angle. The correlation of the ELF emissions with the IMF clock angle is not as strong as with the local shear. Because the wave is best correlated with local quantities, such as shear angle and electron plasma beta, instead of global parameters, it is most likely to be generated locally and not at a distance. Most wave energy is carried by the magnetic field of the wave. The electric field carries little wave energy.

There is no clear evidence that these waves are correlated to the electron temperature anisotropy. Strong enhancements of the waves can occur when the parallel electron temperature is greater than the perpendicular temperature, which makes it unlikely that the waves are driven by the electron temperature anisotropy instability.

There is a clear correlation between the broadband ELF enhancement and the electron plasma beta. There are two possible interpretations. One is that the instability that generates the wave depends on beta, so that the higher the beta is, the stronger the wave is. However, the following is equally possible. The waves are generated by an instability, then heat the particles, and lead to a higher temperature and hence a higher beta. The field shear may be closely related to the beta, as in the field reversal region, and the field strength tends to be weaker, leading to a greater beta. The causal relationship among the three, i.e., field shear, beta, and wave power, is not clear yet.

Statistically, the dispersion relation from the lower hybrid frequency to the electron cyclotron frequency has the characteristics of the whistler mode, but there is a quantitative difference. The cause of this difference is not well understood. Below the lower hybrid frequency the electric wave power drops at the lowest frequencies. Since the lower hybrid waves are mostly electrostatic and are stabilized when the electron plasma beta is high [e.g., *Gary*, 1993], the high power in the magnetic component of the fluctuations and the possible positive correlation with the beta make it unlikely that these waves are lower hybrid modes.

In one case, when the high time resolution data are available, using the spin modulation method, the electric field

of the ELF waves appears to be near perpendicularly polarized with respect to the background magnetic field. Previously, *Gurnett et al.* [1979] investigated spin modulation to study wave polarization. They found few cases that show such spin modulation. We also noted in our study that not every high sampling rate case shows clear spin modulation. One possible explanation for this is the following. If the wave is polarized in the plane perpendicular to the background field, which is often either parallel or antiparallel to the satellite spin axis, the spin modulation cannot be seen because the spin plane and the polarization plane are parallel. The case we present in Figure 15 is when the background field consists of a dominant y_{sc} component, and hence the possible polarization plane is orthogonal to the spin plane. In some cases, either the background field or the wave power itself changes rapidly in the current layer. The spin modulation will not be seen clearly in the signals. The spin modulation effects deserve further comprehensive investigation, so that more information can be obtained about the polarization of these waves.

Acknowledgments. We would like to thank Peter Gary and Bruce Tsurutani for helpful discussions. The work at UM was supported by the National Science Foundation/Office of Naval Research, under award NSF-ATM 9713492 and by the National Aeronautics and Space Administration under cooperative agreement NCCS5-146. The work at UCLA was supported by NASA under research grants NAGW-3948 and NAGW-3974 and by the NSF under grant ATM94-13081. The work at HAO was supported by NASA research grants W-18,582. Work at IOWA was supported by NASA under grant NAG5-7187 with GSFC.

The Editor thanks Dan Winske and Gurbax Lakhina for their assistance in evaluating this paper.

References

Anderson, R. R., C. C. Harvey, M. M. Hoppe, B. T. Tsurutani, T. E. Eastman, and J. E. Etchero, Plasma waves near the magnetopause, *J. Geophys. Res., 87*, 2087, 1982.

Ashour-Abdalla, M., T. Chang, and P. Dusenbery (Eds.), *Space Plasmas: Coupling Between Small and Medium Scale Processes, Geophys. Monogr, Ser.*, vol. 86, AGU, Washington, D.C., 1995.

Drake, J. F., Magnetic reconnection: A kinetic treatment, in *Physics of the Magnetopause, Geophys. Monogr. Ser.*, vol. 90, edited by P. Song, B. U. O. Sonnerup, and M. F. Thomsen, p. 155, AGU, Washington, D.C., 1995.

Drake, J. F., R. G. Kleva, and M. E. Mandt, Structure of thin current layers: Implications for magnetic reconnection, *Phys. Rev. Lett., 73*, 1251, 1994.

Gary, S. P., *Theory of Space Plasma Microinstabilities*, Cambridge Univ. Press, New York, 1993.

Gary, S. P., and T. E. Eastman, The lower hybrid drift instability at the magnetopause, *J. Geophys. Res., 84*, 7378, 1979.

Gurnett, D. A., F. L. Scarf, R. W. Fredricks, and E. J. Smith, The ISEE 1 and ISEE 2 plasma wave investigation, *IEEE Trans. Geosci. Electron., GE-16*, 225, 1978.

Gurnett, D. A., et al., Plasma wave turbulence at the magnetopause: Observations from ISEE 1 and 2, *J. Geophys. Res., 84*, 7043, 1979.

Horwitz, J. L., N. Singh, and J. L. Burch (Eds.), *Cross-Scale Coupling in Space Plasmas, Geophy. Monogr. Ser.*, vol. 93, AGU, Washington, D.C., 1996.

Huba, J. D., N. T. Gladd, and J. F. Drake, On the role of the lower hybrid drift instability in substorm dynamics, *J. Geophys. Res., 86*, 5881, 1981.

Kennel, C. F., and M. Ashour-Abdalla, Electrostatic waves and the strong diffusion of magnetosphere electrons, in *Magnetosphere Plasma Physics*, editing by A. Nishida, p. 245, D. Reidel, Norwell, Mass., 1982.

Kennel, C. F., and H. E. Petschek, Limit on stably trapped particle fluxes, *J. Geophys. Res., 71*, 1, 1966.

Kennel, C. F., F. L. Scarf, R. W. Fredricks, J. H. McGehee, and F. V. Coroniti, VLF electric field observations in the magnetosphere, *J. Geophys. Res., 75*, 6136, 1970.

Kurth, W. S., M. Ashour-Abdalla, L. A. Frank, C. F. Kennel, D. A. Gurnett, D. D. Sentman, and B. G. Burke, A comparison of intense electrostatic waves near f_{UHR} with linear instability theory, *Geophys. Res. Lett., 6*, 487, 1979.

LaBelle, J., et al., AMPTE IRM observations of waves associated wi flux transfer events in the magnetosphere, *J. Geophys. Res., 9* 5827, 1987.

Le, G., C. T. Russell, and J. T. Gosling, Structure of the magnetopause for low Mach number and strongly northward IMF, *J. Geophys. Res., 99*, 23, 723, 1994.

Lemons, D. S., and S. P. Gary, Electromagnetic effects on the modified two-stream instability, *J. Geophys. Res., 82*, 2337, 1977.

Ogilvie, K. W., and R. J. Fitzenreiter, The Kelvin-Helmholtz instability at the magnetopause and inner boundary layer surface, *J. Geophys. Res., 94*, 15,113, 1989.

Ogilvie, K. W., J. D. Scudder, and H. Doong, The electron spectrometer on ISEE 1, *IEEE Trans. Geosci. Electron., GE-16*, 261, 1978.

Petrinec, S., P. Song, and C. T. Russell, Solar cycle variations in the size and shape of the magnetopause, *J. Geophys. Res., 96*, 7893, 1991.

Russell, C. T., The ISEE 1 and 2 fluxgate magnetometers, *IEEE Trans. Geosci. Electron., GE-16*, 239, 1978.

Russell, C. T., and R. C. Elphic, ISEE observations of flux transfer events at the dayside magnetopause, *Geophys. Res. Lett., 6*, 33, 1979.

Shue, J.-H., J. K. Chao, H. C. Fu, C. T. Russell, P. Song, K. K. Khurana, and H. Singer, A new functional form to study the solar wind control of magnetopause size and location, *J. Geophys. Res., 102*, 9497, 1997.

Smith, E. J., and B. T. Tsurutani, Magnetosheath lion roars, *J. Geophys. Res., 81*, 2261, 1976.

Smith, E. J., R. E. Holzer, and C. T. Russell, Magnetic emissions in the magnetosheath at frequencies near 100 Hz, *J. Geophys. Res., 74*, 3027, 1969.

Song, P., R. C. Elphic, and C. T. Russell, ISEE 1 and 2 observations of the oscillating magnetopause, *Geophys. Res. Lett., 15*, 744, 1988.

Song, P., C. T. Russell, and C. Y. Huang, Wave properties near the subsolar magnetopause: Pc 1 waves in the sheath transition layer, *J. Geophys. Res., 98*, 5907, 1993a.

Song, P., C. T. Russell, D. J. Fitzenreiter, J. T. Gosling, M. F. Thomse D. G. Mitchell, S. A. Fuselier, G. K. Parks, R. R. Anderson, and Hubert, Structure and properties of the subsolar magnetopause fo northward IMF: Multiple instrument particle observations, *J. Geophys. Res., 98*, 11,319, 1993b.

Treumann, R. A., J. LaBelle, and T. M. Bauer, Diffusion processes: An observational perspective, in *Geophy. Monogr. Ser.*, vol. 90, *Physics of the Magnetopause*, P. Song, B. U. O. Sonnerup, and M. F. Thomsen eds., 331, 1995.

Tsurutani, B. T., et al., Wave-particle interactions at the magnetopause: Contributions to the dayside aurora, *Geophys. Res. Lett., 8*, 183, 1981.

Tsurutani, B. T., A. L. Brinca, E. J. Smith, T. Okada, R. R. Anderson, and T. E. Eastman, A statistical study of ELF-VLF plasma waves at the magnetopause, *J. Geophys. Res., 94*, 1270, 1989.

Tsurutani, B. T., et al., Broadhand plasma waves observed in the polar cap boundary layer: Polar, *J. Geophys. Res., 103*, 17,351, 1998.

Winske, D., and N. Omidi, Diffusion at magnetopause: Hybrid simulations, *J. Geophys. Res., 100*, 11,923, 1995.

Zhu, Z., P. Song, J. F. Drake, C. T. Russell, R. R. Anderson, D. A. Gurnett, K. W. Ogilvie, and R. J. Fitzenreiter, The relationship between ELF-VLF waves and magnetic shear at the dayside magnetopause, *Geophys. Res. Lett., 23*, 773, 1996.

R. R. Anderson and D. A. Gurnett, Department of Physics and Astronomy, University of Iowa, Iowa City, IA 52242.

K. W. Ogilvie, NASA Goddard Space Flight Center, Code 692, Greenbelt, MD 20771.

C. T. Russell and R. J. Strangeway, Institute of Geophysics and Planetary Physics, University of California, Los Angeles, CA 90095.

P. Song, Space Physics Research Laboratory, University of Michigan, 2455 Hayward Street, Ann Arbor, MI 48109-2143. (psong@umich.edu)

Z. Zhu, High Altitude Observatory, National Center for Atmospheric Research, Boulder, CO 80307.

(Received February 10, 1998; revised June 3, 1998;
accepted July 9, 1998.)